Title: Comparison of Aristolochic acid I derived DNA adduct levels in human renal toxicity models

Authors: Heinke Bastek, Tabea Zubel, Kerstin Stemmer, Aswin Mangerich, Sascha Beneke, Daniel R. Dietrich

PII: S0300-483X(19)30073-3
DOI: https://doi.org/10.1016/j.tox.2019.03.013
Reference: TOX 52193

To appear in: *Toxicology*

Received date: 23 January 2019
Revised date: 22 March 2019
Accepted date: 28 March 2019

Please cite this article as: Bastek H, Zubel T, Stemmer K, Mangerich A, Beneke S, Dietrich DR, Comparison of Aristolochic acid I derived DNA adduct levels in human renal toxicity models, *Toxicology* (2019), https://doi.org/10.1016/j.tox.2019.03.013

Comparison of Aristolochic acid I derived DNA adduct levels in human renal toxicity models

Heinke Bastek[1*], Tabea Zubel[2*], Kerstin Stemmer[3], Aswin Mangerich[2], Sascha Beneke[1], Daniel R. Dietrich[1$]

[1] Human and Environmental Toxicology, University of Konstanz, Konstanz, Germany

[2]Molecular Toxicology, University of Konstanz, Konstanz, Germany

[3] Division of Pharmacology and Toxicology, Institute for Diabetes and Obesity, Helmholtz Zentrum München, Neuherberg, Germany

[$] Corresponding author

[*] Equal contribution

Address all correspondence and requests for reprints to:

Daniel R. Dietrich, Human and Environmental Toxicology, University of Konstanz, Universitätsstraße 10, 78464 Konstanz, Germany.

Email: daniel.dietrich@uni-konstanz.de

Phone: +49-7531-88-3518

Abstract

Aristolochic acid (AA) dependent human nephropathy results either from environmental exposure to *Aristolochiaceae* plant subspecies or their use in traditional phytotherapy. The toxic components are structurally related nitrophenanthrene carboxylic acids, *i.e.* Aristolochic acid I (AAI) and II (AAII). AAI is considered to be the major cause of Aristolochic acid nephropathy, characterized by severe renal fibrosis and upper urothelial cancer. Following enzymatic activation in kidney and/or liver, AAI metabolites react with genomic DNA to form persistent DNA adducts with purines. To determine whether AAI can be activated in human renal cells to form DNA adducts, we exposed telomerase immortalized renal proximal tubular epithelial cells (RPTEC/TERT1), the human embryonic kidney (HEK293) cell line, as well as primary human kidney cells (pHKC) to AAI *in vitro*. We modified an isotope dilution ultra-performance liquid chromatography/tandem mass spectrometry (ID-UPLC-MS/MS) based method for the quantification of dA-AAI adducts in genomic DNA. In addition, time dependent accumulation of adducts in renal cortex and bladder tissue from AAI/II treated Eker rats were used to validate the detection method. AAI-induced toxicity in human renal cells was determined by dA-AAI adduct quantification, the impact on cell viability, and NQO1 expression and activity. Our findings demonstrated adduct formation in all cell lines, although only pHKC and RPTEC/TERT1 expressed NQO1. The highest adduct formation was detected in pHKC despite low NQO1 expression, while we observed much lower adduct levels in NQO1-negative HEK293 cells. Adduct formation and decreased cell viability correlated only weakly. Therefore, our data suggested that *i.)* enzymes other than NQO1 could be at least equally important for AA bioactivation in human renal proximal tubule cells, and *ii.)* the suggested correlation between adduct levels and viability appears to be questionable.

Keywords:

Aristolochic acid, DNA adducts, UPLC-MS/MS, NQO1, human kidney cells

1. Introduction

Aristolochic acids (AA) are a group of structurally related nitrophenanthrene carboxylic acids and have been detected in several *Aristolochiaceae* and *Asarum* plant subspecies, also known as birthwort or pipevine (Debelle et al., 2008). The major AA derivatives contained in the plant extract of *Aristolochia* species are Aristolochic acids I (AAI) and II (AAII). Human kidney diseases associated with AA exposure are summarized under the term "Aristolochic acid nephropathy" (AAN), caused either by ingestion of plants containing AA as part of traditional phytotherapies (formerly known as "Chinese herbs nephropathy"), or by the environmental contaminants in food (Balkan endemic nephropathy) (Jadot et al., 2017). The pathology of AAN in humans is basically characterized by extensive cortical tubular atrophy, loss of tubules and dense interstitial fibrosis, most prominent in the outer area of the cortex, while the glomeruli are relatively spared (Jelakovic et al., 2011, Depierreux et al., 1994). Progressive renal fibrosis results in loss of function and subsequently to end stage renal disease and kidney failure, requiring dialysis or transplantation. AAN patients are also frequently diagnosed with urothelial (transitional cell) carcinomas of the renal pelvis and ureter (Cosyns, 2003). These upper urinary tract cancers (UUCs), which account for only 5% of all urinary tract cancers worldwide, are present in ~50% of AAN cases (Nortier et al., 2000).

In contrast, in rodents, employed as surrogate species for understanding the mechanisms underlying AA induced toxicity, nephropathy and carcinogenesis do not readily reflect the pathologies observed in humans. Indeed, the observed pathologies appear to differ dramatically dependent on whether AA exposure occurred via subcutaneous, intraperitoneal application or via oral gavage. Mice and rats exposed acutely and chronically to AAI via gavage developed

ulceration in the forestomach, extensive tubular necrosis and primarily forestomach and renal cortical tumors in absence of renal fibrosis, respectively. Specific rodent strains developed renal fibrosis when treated via subcutaneous or intraperitoneal injection with AAI, as reviewed by Debelle et al (2008). Consequently, metabolic activation of AAI, either in the liver or directly in the renal cortex, appears critical for the development of renal proximal tubule cytotoxicity, inflammation, and ensuing epithelial to mesenchymal transition and fibrosis, whereby the relationship between cytotoxicity and AAI-DNA adducts is not clear to date. Indeed, metabolic activation of AAI leads to a highly reactive intermediate, a nitrenium/carbenium ion, which is able to form DNA adducts including 7-(deoxyadenosine-N^6-yl) aristolactam I (dA-AAI) and 7-(deoxyguanosine-N^2-yl) aristolactam I (dG-AAI) (Pfau et al., 1990). Currently, nitroreduction e.g. by NAD(P)H dehydrogenase (quinone 1) (NQO1) is considered to be the main pathway for AAI bioactivation (Fig. 1) and thus is assumed to be required for AAI-DNA adduct formation in humans (Stiborova et al., 2003). However, other phase I enzymes, abundant in the liver, e.g. the cytosolic nitroreductases (e.g. xanthine oxidases), cytochrome P450s (CYP) enzymes (e.g. CYP1A1, 1A2, or NADPH:CYP reductase) or peroxidases may be involved in AAI metabolism (Stiborova et al., 2005, Stiborova et al., 2009). Thus, one would expect that hepatic activation of AAI leads to cytotoxic AAI-intermediates capable of forming DNA adducts and therefore to observable hepatotoxicity and/or DNA-adducts in hepatocytes. Contrary to expectations, patient derived material demonstrated no overt hepatotoxicity. However, the liver and other organs of an AAI exposed patient (spleen, lung, adrenal, stomach, small intestine, bladder, lymph nodes, pancreas, brain) exhibited similar, lower or higher DNA-adduct level (expressed as relative adduct labeling using ^{32}P-postlabelling and expressed as mean dA-AAI adducts per 10^9 nucleotides) compared to the corresponding kidney of the same patient (Arlt et al., 2004, Nortier et al., 2003). The mean relative dA-AAI adduct levels reported in the renal cortex of male and female patients ranged between 30 - 3880 dA-AAI adducts per 10^9 nucleotides analyzed using UPLC-MS/MS (Yun et al., 2012). Although less accurate, dA-

AAI adducts were also frequently quantified in kidney samples using ^{32}P-postlabeling and ranged between 1 - 2340 (Arlt et al., 2004, Nortier et al. 2003, Yun et al., 2012). Due to their long persistence, the specific DNA adducts in patients can serve as biomarkers of exposure to AAI (Stiborová et al., 2017). However, most likely the presence of DNA adducts are of little help for a better understanding of AA bioactivation and thus of the development of AAI mediated renal proximal cytotoxicity and ensuing nephropathy, as these adducts *per se* can be detected also in organs without pathological changes.

In order to address several of the questions raised above, we used male and female Eker rats exposed daily to a mixture of AAI and AAII to establish and validate an isotope dilution (ID)-UPLC-MS/MS state-of-the-art quantification method for dA-AAI adduct levels based on the method previously published by Yun et al. (2012). AAI exposure mediated dA-AAI adduct levels were determined in renal tissues of exposed rat and humans, but not compared to *in vitro* settings. Therefore, we employed this dA-AAI adduct detection and quantification method to determine AAI derived DNA adduct formation not only in renal cortex and bladder of exposed Eker rats, but also in human renal *in vitro* cell systems. For this we employed human embryonic kidney (HEK293) cells, representing a viral immortalized cell model, proliferating or differentiated hTERT immortalized human renal proximal tubular epithelial cells (RPTEC/TERT1) (Wieser et al., 2008), and differentiated primary human kidney cells (pHKC). Finally, we compared dA-AAI adduct formation to AAI-induced reduction in cell viability and examined the expression and activity of NQO1 relevant for AAI-bioactivation.

Material and methods

2.1 Materials

Aristolochic acid I (AAI) and the AA sodium salt mixture (41% AAI and 56% AAII) were purchased from Sigma-Aldrich. [$^{15}N_5$]-labeled 2'-deoxyadenosine ([$^{15}N_5$]-dA) was purchased

from Cambridge Isotope Laboratories, Inc. 2'-deoxyadenosine, calf thymus DNA, DNase I (Type IV, from bovine pancreas), alkaline phosphatase (*Escherichia coli*), nuclease P1 (*Penicillium citrinum*), phosphodiesterase I (*Crotalus adamanteus* venom), NADPH, menadione and formic acid (LC-MS grade) were purchased from Sigma-Aldrich. Thiazolyl blue (MTT), dimethyl sulfoxide (DMSO) (>99,98 %) and *N*,*N*-dimethylformamide (DMF) (>99,8 %) were purchased from Roth. All solvents for mass spectrometry were of LC-MS grade from Roth.

2.2 Rodent experiments

Six to ten weeks old heterozygous *Tsc2* mutant Eker rats (*Tsc2*$^{+/-}$, Long Evans) were purchased from the MD Anderson Cancer Center, Smithville, Texas, USA and housed at the University of Konstanz animal research facility under standard housing conditions. Prior to exposure, male and female Eker rats were randomly assigned to dose groups and allowed to acclimatize to laboratory conditions for 4 weeks. All animal experiments were approved by the State of Baden-Württemberg, Germany (Regierungspräsidium Freiburg, AZ: G-03/65). Groups of three male and female Eker rats were treated daily by oral gavage with a mixture of AAI (41%) and AAII (56 %) for 1, 3, 7, and 14 days (10 mg / kg bodyweight). Time-matched vehicle controls (n=3) received corresponding volumes of 0.1 M $NaHCO_3$. Rats were weighed daily. At the end of each treatment period, anesthetized rats were sacrificed by exsanguination subsequent to retrograde perfusion with PBS. Organs were collected, sliced and sections were snap frozen and stored at -80 °C until further usage.

2.3 Routine cell culture

All cells were cultured routinely in T75 flasks (Sarstedt) at 37 °C in a 5 % CO_2 humidified atmosphere and subcultured by trypsinization. Fresh medium was provided three times per week. The human proximal tubule cell line RPTEC/TERT1 (Wieser et al., 2008) were

purchased from Evercyte GmbH, Vienna, Austria and cultured in hormonally defined medium consisting of a 1 to 1 mixture of Dulbecco's modified Eagle's medium (Life Technologies, Darmstadt, Germany) and Ham's F-12 nutrient mix (Life Technologies) supplemented with 2 mM Glutamax (Life Technologies), 5 µg/ml insulin (Sigma), 5 µg/ml transferrin (Sigma), 5 ng/ml sodium selenite (Sigma), 10 ng/ml epithelial growth factor (Sigma) and 36 ng/ml hydrocortisone (Sigma), 100 U/ml penicillin and 100 µg/ml streptomycin. For subculturing, cells were seeded at 30 % density and harvested or treated at day 3-4 (80-90 % confluence) for proliferating cells or at day 16 for differentiated cells. Proliferating (day 3-4) and differentiated (day 16) RPTEC/TERT1 cells reflect radically different phenotypes (Aschauer et al., 2013). For transwell experiments the cells were seeded at 100 % density on PET transwell® inserts with 0.4 µm pore size (Corning) and harvested or treated after 10 days post-initial seeding. Human embryonic kidney cells HEK293 were purchased from the Leibniz Institute *DSMZ – German Collection of Microorganisms and Cell Cultures* and cultured in Dulbecco's modified Eagle's medium (DMEM) containing low glucose (1g/l) supplemented with 10 % fetal bovine serum (FBS) gold, 100 U/ml penicillin and 100 µg/ml streptomycin. Cells were seeded at a density of 5 x 10^4 cells/cm^2 on poly D-Lysine (Sigma-Aldrich) coated plates and harvested or subjected to treatment 48 h later.

Primary human renal epithelial cells (pHKC) were isolated from human biopsy material (Klinikum Konstanz, Konstanz, Germany) from a 65 year old woman as described by O'Brien et al. (2001). Cells were cultured in DMEM/Ham's F-12 (Biochrom) supplemented with 1 x Insulin-Transferrin-Selenium (ITS-G) (Invitrogen), 10 ng/ml epidermal growth factor (Sigma), 18 ng/ml hydrocortisone (Sigma), 4 ng/ml L-thyroxin (Sigma), 100 U/ml penicillin and 100 µg/ml streptomycin. Cells were seeded at a density of 0.5-1 x 10^6 cells/cm^2 and processed further after 48 h incubation (confluent monolayer).

2.4 Cell treatment for DNA adduct detection

Cells were seeded, as mentioned above, in 6 well plates (for DNA extraction), in 96 well plates (for MTT cell viability assay and NQO1 assay) or in 6 well transwell inserts. At day of exposure medium was exchanged with fresh medium containing various concentrations of AAI in 0.2 M $NaHCO_3$ and cells were incubated for additional 48 h at standard conditions.

2.5 Extraction and enzymatic digestion of DNA

DNA from cell and tissue samples was extracted with the PureLink™ Genomic DNA Mini Kit (Thermo Fisher Scientific) according to the manufacturer's protocol. For cellular samples, cells from one well of a 6 well plate were trypsinized, washed and processed according to manufacturer's protocol. For the rat tissue, 40-50 mg tissue were lysed for 1-1.5 h in the genomic digestion buffer before DNA extraction. DNA was finally eluted in 100 µl nuclease free water and DNA concentration was assessed via nanodrop.

The enzymatic digestion conditions used for DNA hydrolysis to 2'deoxynucleosides were adapted from Yun et al. (2012) and Goodenough et al. (2007). DNA (5-10 µg) was diluted to 100 ng/µl H_2O and 2 fmol/µl internal standard ($[^{15}N_5]$-dA-AAI) were added prior digestion. DNase I (2542 U/mL in 0.15 M NaCl; 1016.8 U/mg DNA) was added, and the mixture was incubated for 1.5 h. Next, nuclease P_1 (*Penicillium citrinum*; 100 U/mL in 1 mM $ZnCl_2$; 16 U/mg DNA) was added, and the incubation was further incubated for 3 h at 37 °C. Finally, alkaline phosphatase (*E. coli*; 24 U/mL in 1 mM $MgCl_2$; 8 U/mg DNA) and phosphodiesterase I (*Crotalus adamanteus* venom; 1.7 U/mL in 110 mM Tris-HCl at pH 8.9, containing 110 mM NaCl, 15 mM $MgCl_2$; 0.2856 U/mg DNA) were added last, and the incubation was continued for additional 18 h at 37 °C. After digestion, samples were evaporated to dryness by vacuum centrifugation for 2 h and rehydrated in H_2O for 2 h. Equal volume of DMSO was added to a final concentration of 0.125 ng DNA/µl in 50 % DMSO. Samples were stored at -20 °C and filtered through a 0.2 µm Millex-LG PTFE syringe filter (Millipore) before adduct quantification.

2.6 Synthesis and purification of dA-AL-I standards

The synthesis of dA-AAI and [$^{15}N_5$]-dA-AAI standards were performed by the reaction of AA-I with dA or [$^{15}N_5$]-dA, using a modification of the protocol described by Yun et al. (2012). AA-I (1 mg) in DMF (100 µl) were mixed with 20 mg Zn dust (Sigma), pre-activated with 1 % HCl for 15 min. Then, dA or [$^{15}N_5$]-dA (2 mg) in 50 mM potassium phosphate buffer (1 ml, pH 5.8) were added and incubated at 37 °C for 16 h in the dark while shaking. Thereafter, the solution was placed at 4 °C for 30 min to pellet the Zn dust. The supernatant was removed and the Zn pellet was washed with 2 x 250 µl H_2O. The combined supernatants were applied to Isolute SPE C18(ec) cartridges (500 mg) (Biotage), which were preconditioned with CH_3OH (2 ml), followed by H_2O (2 ml). Subsequently, the cartridges were washed with H_2O (2 x 2 ml). The adducts (together with AA-I, AL-I and residual dA) were eluted with CH_3OH (2 ml) and evaporated to dryness by vacuum centrifugation, finally dissolved in DMSO (250 µl). Purification of standards was performed on a 2695 Alliance Separation Module (Waters) with a Vydac protein & peptide C18 column (300 Å, 5 µm, 4.6 x 250mm). In the first purification step dA-AAI and AL-I (t_R: 31.2 – 32.7 min) were purified with a gradient starting with 90 % buffer A (H_2O supplemented with 0.1% acetic acid) at a flow rate of 0.6 ml/min. Buffer B (acetonitrile supplemented with 0.1% acetic acid) was increased to 90% in 30 min and held constant for 5 min. A second purification step was performed using the same conditions with methanol instead of acetonitrile to purify dA-AAI (t_R: 20.9 – 22.7 min) from AL-I. Final fractions containing dA-AAI and [$^{15}N_5$]-dA-AAI standards were evaporated to dryness using vacuum centrifugation and dissolved in DMSO.

2.7 Validation of chemical standard for mass spectrometric analysis

UV/Vis spectra were acquired with an Ultrospec 2100 pro from Amersham Biosciences. Extinction coefficients were ε_{305}=16,140 l×mol^{-1}×cm^{-1} and ε_{415}=5,400 l×mol^{-1}×cm^{-1} (Yun et al.,

2012). Product ion scans were acquired at a Xevo TQ-S tandem MS from Waters. High-resolution MS of each adduct was performed at a Thermo LTQ Orbitrap Discovery in the Proteomics Facility of the University of Konstanz. NMR spectra were determined with a Bruker Avance III 600 at the NMR core facility of the University of Konstanz.

2.8 Isotope dilution-UPLC-MS/MS quantification

Analysis was performed on an ACQUITY UPLC H-class coupled to a Xevo TQ-S tandem MS (Waters). An ACQUITY UPLC Peptide CSH C18 column (130 Å, 1.7 µm, 2.1 × 50 mm, Waters) was used for chromatographic separation. DNA samples were analyzed with a flow rate of 0.4 ml/min. Mobile phase A was Millipore water and B was acetonitrile (LC-MS grade, Carl Roth), both supplemented with 0.1% formic acid (Sigma-Aldrich). Initial conditions were 90 % A. B was increased to 90 % in 8 min and held for 2 min.

The source settings were: Capillary: 0.7 kV, Cone: 11V, Source Offset: 50 V, Source Temperature: 150 °C, Desolvation Temperature: 500 °C, Cone Gas Flow: 150 l/h, Desolvation Gas Flow: 1000 l/h, Collision Gas Flow: 0.15 ml/min, Nebuliser Gas Flow: 7 bar. The analyzer was set to high mass resolution. The analytes were measured with cone voltage of 6 V, collision energy of 10 V and an auto dwell-time (104 ms) in MRM mode. The transitions $[M+H]^+$ were dA-AAI 543.3 > 427.2 and [^{15}N]-dA-AAI 548.3 > 432.2. DNA amounts were determined by UPLC-MS/MS measurements (estimated injection of 0.6 ng DNA) with the same parameters as described for nucleic acid adducts. The following ion transitions $[M+H]^+$ were analyzed: dG m/z 268.1>152, dA m/z 252>136, dT m/z 243>127 and dC m/z 228>112.

2.9 Validation of the analytical method

Serial dilution of standard stock solutions was performed to determine the linearity and sensitivity. LOD (S/N of 3) and LOQ (S/N of 10) was determined. Quality control samples were prepared in a low, medium and high concentration (LQC, MQC and HQC) of 5, 50 and

500 fmol to determine inter-day and intra-day precision (n=5) according to FDA guidelines (FDA, 1995). Three different sample sets were prepared according to EMA guidelines (European Medicines Agency, 2011) to define recovery and matrix effects: Standards were spiked in digested blank matrix (Set 1), standards were spiked in water (Set 2) or standards were digested in presence of blank matrix (Set 3). Samples were evaporated to dryness using vacuum centrifugation and re-dissolved in 50 % DMSO. The percentage of recovery was calculated by the ratio of the peak areas of Set 3 and 1. The ratio of the peak area of Set 1 and 2 determined matrix effects. All sets (1-3) were normalized to internal standards. The influence of storage was evaluated by short-term storage at RT and 37 °C for 6, 12 and 24 h. The influence of long-term storage at -20 °C and -80 °C was determined after 2 and 4 weeks. Impact of freeze-thaw cycles (1-3 times) was also determined. All storage samples were analyzed in triplicates of all three QC concentrations and normalized to internal standards.

2.10 MTT cell viability assay

Cell viability was determined by MTT reduction assay. Treated cells were incubated with 1 mM MTT in medium at 37 °C for 1 h. MTT was removed and cells were lysed in 95 % isopropanol and 5 % formic acid. Formazan absorption was measured at 550 nm using a Tecan M200Pro microplate reader (Tecan). Values obtained for dead cells (0.1 % Triton X-100) were subtracted from all other values. Viability data were expressed as percentage of non-treated (control) cells.

2.11 Western Blot analysis

One well of a 6 well plate was used for protein sample preparation for each cell line. Cells were trypsinized, washed in PBS and lysed with 200-300 µl RIPA buffer (50 mM Tris-HCl, 150 mM NaCl, 0.1 % SDS, 0.5 % sodium deoxycholate, 1 % Triton X-100) for 10 min on ice. After passage through a 26G needle, protein concentrations were determined using Pierce BCA Protein Assay (Thermo Fisher Scientific) and samples for SDS Page were generated by addition

of 1.5 X Urea sample buffer (93.75 mM Tris-HCl pH=6.8, 9 M Urea, 7.5 % (v/v) β-mercapto-ethanol, 15 % (v/v) glycerol, 3 % (w/v) SDS, 0.01 % (w/v) bromphenol blue), boiled at 95 °C for 5 min. and stored at -80 °C. Subsequently, 4.5 µg total protein/sample were separated by a 12 % SDS-PAGE and blotted onto a nitrocellulose membrane. Membranes were detected either with Ponceau S and then blocked with 5 % (w/v) milk powder in TTBS (100 mM Tris-HCl, 150 mM NaCl, 0.1 % (v/v) Tween 20, pH 7.6) for 1 h at RT. Proteins of interest were detected either with anti-NQO1 antibody (1:1000 in 5 % milk, Thermo Fisher Scientific, #MA1-16672) or with anti-β-actin (1:4.000 in 5 % milk, Sigma, #A2228) over night at 4 °C. After washing, membranes were incubated for 1 h at RT with peroxidase-conjugated secondary antibody anti-mouse IgG-peroxidase (1:80.000 in 5 % milk, Sigma-Aldrich, #A9044). Signals were detected by enhanced chemiluminescence (Lumigen® ECL ultra, Lumigen) via ImageQuantTM LAS 4000 (GE Healthcare). Stripping of the membrane was performed with 0.2 M NaOH for 10 min followed by incubation for 10 min in Millipore H_2O.

2.12 NQO1 activity assay

NQO1 activity assay was performed using a modified protocol of the “Prochaska” microtiter plate bioassay described by Fahey et al. (2004). For determination of NQO1 induction after AAI exposure, cells were treated with solvent control, AAI in 0.2 M $NaHCO_3$ or 5 µM sulforaphane in DMSO for 48 h. Cells were washed with PBS and lysed by incubation with 50 µl 0.8 % digitonin in 2 mM EDTA (pH 7.8) at 37 ℃ for 10 min followed by an additional incubation at 25 °C for 10 min while shaking. For transwell inserts cells were detached by trypsinization, washed and lysed in 750 µl 0.8 % digitonin in 2 mM EDTA (pH 7.8). Briefly, 10 µl cell lysates were transferred into a 96 well plate and mixed with 200 µl of the reaction mixture containing 25 mM Tris-HCl (pH 7.4), 0.066 % bovine serum albumin, 0,01 % Tween-20, 7.2 µM MTT, 1 mM NADPH (freshly added) and 50 nM menadione (freshly added). Control reactions were performed by addition of 50 µl 0.3 mM dicoumarol in 0.5 % DMSO

and 5 mM potassium phosphate (pH 7.4). Blank reactions were performed w/o menadione in the reaction buffer. Absorption was quantified at 610 nm every min for 30 min in total using a Tecan M200Pro microplate reader. The specific NQO1 activity was quantified using the slope of the linear range of absorption increase. Values were normalized to total protein amount, quantified by Pierce^{TM} BCA Protein Assay Kit.

2.13 Statistical analysis

Unless otherwise indicated data are presented as mean ± SEM. Sample size (*n*) indicates the number of independent experiments performed. Statistical significance was determined using GraphPad Prism 7, statistical tests as indicated in the figure legends.

2. Results

3.1 Performance of the UPLC-MS/MS detection method of dA-AAI adducts

AAI derived DNA adducts are considered relevant and reliable biomarkers for AAI exposure, whereby dA-AAI (Fig. 1) represents the predominant adduct found in animal and patient material. As isotope-dilution LC-MS/MS is considered the gold standard for quantification of DNA adducts, dA-AAI and [$^{15}N_5$]-dA-AAI standards were synthesized with a modified biomimetic reaction described earlier by Yun et al. (2012). Pre-purification of standards was performed by solid phase extraction (SPE). Final purification was achieved via HPLC with an approximate yield of ~1-1.5 % compared to the AAI starting material. dA-AAI and [$^{15}N_5$]-dA-AAI standards were verified by their characteristic UV/Vis spectra (Fig. S-1), product ion scans (Fig. 2 a and b), high resolution MS (Fig. S-2), ^{1}H-NMR (Fig. S-3 and S-4) and 2D-NMR (Fig. S-5). Product ion scans resulted in detection of the aglycone adducts ([BH_2]$^+$ of dA-AAI *m/z* 427 and for [BH_2]$^+$ of [$^{15}N_5$]-dA-AAI *m/z* 432) (Fig. 2 c), which were subsequently used for quantification with ID-UPLC-MS/MS. The sensitivity was determined at a limit of detection

(LOD, S/N of 3) of 0.1 fmol and a limit of quantification (LOQ, S/N of 10) of 0.5 fmol (Table 1). Serial dilutions of unlabeled standard, spiked with internal isotopically labeled standard were used to prepare a calibration curve (Fig. 2 d and Table 1) with a linear range of at least three orders of magnitude from 0.5 fmol to 1000 fmol (R^2 = 0.9926). Representative chromatograms of treated and control samples are shown in Fig. 2 e, f. Peak areas for dA-AAI and [$^{15}N_5$]-dA-AAI were analyzed at a retention time of 4.2 minutes.

According to the EMA guidelines (European Medicines Agency, 2011), recovery and matrix effects were determined (Table 2). Recovery rates were determined by comparing standards, which were digested together with blank matrix, to standards which were spiked to separately digested blank matrix. Matrix effects were determined by standards spiked to digested blank matrix compared to standards spiked into water. All values were found to be within the acceptable limits as suggested by EMA (European Medicines Agency, 2011). Quality controls (QC) were prepared over a low (LQC), medium (MQC), and high (HQC) concentration range of 5, 50 and 500 fmol. The values of percent relative standard deviation (% RSD), which is a measure for the precision of a method, were < 20 % for LQCs and < 15 % for MQCs and HQCs for samples measured on the same day (intra-day precision) and on different days (inter-day precision). These values were fully compatible with FDA guidelines for the validation of analytical procedures (FDA, 1995). Potential analyte loss due to storage or repeated freeze-thaw cycles was determined (Table 3). Short-term storage at ambient temperatures (RT and 37 °C), as well as long-term storage at lower temperatures (-20 °C and -80°C) had no influence on measurement of the analyte. Taken together a reliable, robust, sensitive and accurate ID-UPLC-MS/MS method was established to quantify dA-AAI adducts from cells exposed *in vitro*.

3.2 UPLC-MS/MS analysis of dA-AAI adduct formation in fresh frozen rat tissue

We analyzed dA-AAI adduct formation in kidney cortex (Fig. 3 a, b) and bladder (Fig. 3 c, d) tissue from AAI/II exposed male and female Eker rats (10 mg / kg bodyweight per day). We were able to detect dA-AAI adduct formation already 24 h after oral exposure and observed a time-dependent accumulation of DNA adducts in the kidney cortex and in bladder. Based on the adduct curves in renal cortex, it appeared that male Eker rats had greater AAI activation and thus DNA adduct formation than their female counterparts. Additionally, male Eker rats displayed a severe reduction in bodyweight (Fig. 3 e), whereas AAI/II treated female Eker rats showed only a decrease in bodyweight gain compared to the control group (Fig. 3 f). In contrast to the renal cortex, DNA adduct levels in the bladder were approximately ten times lower and showed no sex differences.

3.3 Comparison of dA-AAI adduct formation in human primary and immortalized renal cells

Based on the verification of dA-AAI adduct detection in rat tissue, we used our ID-UPLC-MS/MS protocol to quantify DNA adduct formation in two different human renal cell lines (HEK293 and RPTEC/TERT1) and primary human kidney cells (pHKC). Cells were exposed to different AAI concentrations (1-100 µM) or solvent control for 48 h. We observed a concentration dependent increase in dA-AAI adduct levels in all cells (Fig. 4 a). However, DNA adduct levels appeared to reach saturation in pHKC already at very low AAI exposure concentrations, whereas this was not observable in differentiated RPTEC/TERT1 or in HEK293 cells. The comparison of pHKC and HEK293 cells provided for an approximately 100-fold difference in DNA-adducts quantified. When considering the 3 x 10^9 base pairs per diploid genome in a human cell, the DNA adducts detected can be expressed as DNA adducts per cell. Thus, the “saturation” in DNA adducts as observed is apparently either the result of cell type specific saturable enzymatic activation capabilities and/or a saturation of available dA and dG sites that are “adductable”. Alternatively, different cell lines may tolerate different adduct levels at which cell death occurs (see below).

To assess the impact of cell differentiation on dA-AAI adduct formation, proliferating (day 3) and differentiated (day 16) RPTEC/TERT1 cells on 2D wells and RPTEC/TERT1 cells grown on transwell-inserts (day 10) were exposed to the same AAI concentration range (Fig. 4 b). Adduct levels increased rapidly in differentiated compared to proliferating RPTEC/TERT1, while proliferating RPTEC/TERT1 and RPTEC/TERT1 cultured on transwell inserts showed a similar concentration response in adduct levels.

3.4 Influence of AAI exposure on cell viability

The effect of AAI on cell viability, as assessed via MTT reduction assay after 48 h exposure to various AAI concentrations (Fig. 4 c), demonstrated an AAI concentration dependent loss of cell viability, but also large differences in susceptibility amongst the three different cell types. pHKC were most sensitive to AAI, showing a loss of viability already at 1 µM and a near maximal loss of viability 10 µM AAI, *i.e.* the same concentration where DNA adduct levels reached near saturation levels (Fig. 4 a). Conversely, RPTEC/TERT1 cells were much more resistant to AAI, where demonstrable reduction of viability (70 % compared to ctrl.) was observable as of 100 µM AAI, despite that DNA adducts were 5-fold higher than in pHKC at 1 µM with similar reduction in viability (Fig 4 d). HEK293 cell viability was similar to the one observed for differentiated RPTEC/TERT1 cells, albeit at higher AAI concentrations (>100 µM) HEK293 cells appeared to be more sensitive than RPTEC/TERT1 cells (Fig. 4 c). The comparison of cell viability with DNA adducts on a cell type basis (Fig. 4 d) demonstrated that a 5x and 25x lower number of DNA adducts were required in HEK293 cells to reduce cell viability than was the case for differentiated pHKC and RPTEC/TERT1 cells, respectively. Obviously, issues e.g. expression of organic anion transporter 1 (OAT1), known to be important for AAI uptake (Dickman et al., 2011, Xue et al., 2011), as well as level of expression of phase II enzymes (e.g. glutathione transferase (GST)) and levels of cytosolic glutathione, but not of phase I enzymes (e.g. NQO1) will play a major role.

3.5 Comparison of NQO1 expression and activity in HEK293, RPTEC/TERT1 and pHKC

As noted earlier NQO1 is considered central in the metabolic activation of AAI and thus the formation of DNA adducts. Accordingly, we examined the expression and the relative activity of NQO1 in the three different cell types employed. As demonstrated (Fig. 5 a), HEK293 cells do not express NQO1, and only a small amount of NQO1 can be detected for the differentiated pHKC cells. Differentiation and/or the culturing technology appeared not to play a major role with regard to NQO1 expression in RPTEC/TERT1, as demonstrated when NQO1 expression levels were normalized to the housekeeping gene β-actin (Fig. 5 b). However, RPTEC/TERT1 cells displayed a significantly higher level of expression than pHKC cells. As level of expression bears no information as to whether or not NQO1 is enzymatically active, NQO1 activity (Fig. 5 c) was assessed using a modified version of the "Prochaska" microtiter assay (Fahey et al., 2004) or normalized to NQO1 expression levels (Fig. 5 d). In sum, NQO1 expression and activity was much higher in RPETC/TERT1 cells compared to pHKC cells, while expression levels and activity of NQO1 in HEK293 were not significantly distinguishable from background.

3.6 Lack of AAI mediated NQO1 induction in HEK293, RPTEC/TERT1 and pHKC

Currently, it is assumed that NQO1 can be induced by AAI exposure (Bárta et al., 2014), suggesting that exposure to AAI would induce its own bioactivation *in situ*. To address the latter, we determined NQO1 activity subsequent to 48 h exposure to AAI (1-100 µM), solvent control, or 5 µM sulforaphane. Sulforaphane, a broccoli-derived phytochemical, was demonstrated to activate Nrf2 and thus increased expression of NQO1 (Houghton et al., 2016). Contrary to previous reports, AAI exposure did not induce an increased expression of NQO1 in any of the cells tested. However and as expected, sulforaphane treatment resulted in a significant increase in NQO1 activity in differentiated RPTEC/TERT1 cells (Fig. 6 a) and

pHKC (Fig. 6 b), but not in HEK293 (Fig. 6 c) cells, thus corroborating the absence of constitutive and inducible NQO1 expression in HEK293 cells.

3. Discussion

Although ^{32}P-postlabeling is a commonly used technique for investigating AA mediated formation of DNA adduct formation in experimental animal models (Dong et al., 2006) and patients with nephropathy (Yun et al., 2012, Bieler et al., 1997), ^{32}P-postlabeling encompasses several limitations, e.g. variable labeling efficiencies, equivocal identities of carcinogen adducts, semi-quantitative assessment, low through-put etc. Similarly, the use of antibodies for detection of dA-AL I adducts (Chang et al., 2017) via secondary antibodies labeled with fluoro- or chromophores, have similar limitations, e.g. sensitivity, semi-quantitative assessment, low through-put and, most importantly, yet still lacks direct structural validation of detection using DNA adduct quantification with stable, isotopically labelled internal standards. Modern techniques e.g. LC-MS/MS represents a more reliable method to quantify AA derived DNA adducts (Yun et al., 2012) that is also applicable to difficult samples such as paraffin-embedded tissue and implementation for high through-put (Yun et al., 2017). As to date AAI mediated DNA-adducts were not determined in the *in vitro* settings, we adapted the previously published protocol by Yun et al. (2012, 2017) to our settings. By employing a *de novo* synthetized internal standard for adducts, i.e. ion scan, high resolution MS, NMR and UV/Vis spectra characterized unlabeled and stable isotope labeled ([$^{15}N_5$]-) dA-AAI (Fig. S-1 – S-5), we established a highly sensitive ID-UPLC-MS/MS method. The use of the internal standard allows detection of sample loss during preparation and variances during measurements, resulting in reduced variability in the data. This highly sensitive ID-UPLC-MS/MS method was validated with regard to linearity, recovery, matrix effects, precision, and storage conditions according to FDA and EMA guidelines and was demonstrated to allow quantification of AAI mediated DNA-adducts in rat

renal and bladder tissues as well as in *in vitro* exposed HEK293, proliferating and differentiated RPTEC/TERT1 and pHKC cells. The comparison of our ID-UPLC-MS/MS method with the previously published approach by Yun et al. (2012, 2017), reporting an LOQ of 0.3 dA-AAI adducts per 10^8 DNA bases which corresponds to 0.0917 fmol, demonstrated similar sensitivity (LOD 0.1 fmol; LOQ: 0.5 fmol).

To evaluate our established method for dA-AAI quantification we analyzed the dA-AAI adduct levels in Eker rats, orally exposed (1, 3, 7 or 14 days) to a mixture of AAI and II (10 mg / kg bodyweight). In line with the published persistence of adducts in patient (Stiborová et al., 2017) due to their ability to evade global genome repair (Sidorenko et al., 2012), we observed a time dependent accumulation of dA-AAI adducts in rat renal cortex and bladder. Adduct levels in renal cortex were ten times higher than in bladder tissue. Previous studies reported that renal cortex from the very same rats did not display necrosis or increased cell proliferation, but upregulation of NQO1 and several p53 dependent pathway genes, suggestive of a DNA damage response (Stemmer et al., 2007). Furthermore, our data confirmed dA-AAI adduct levels reported by Yun et al. (2012) in the kidney (1020 dA-AAI adducts/10^8 bases) for mice treated with 1 mg/kg (unknown duration) (Yun et al., 2012). Unfortunately, no reference values are available for dA-AAI adduct levels detected by UPLC-MS/MS in the bladder.

As we confirmed the applicability of our dA-AAI quantification method, we subsequently investigated AAI toxicity in different human renal cell models. We compared the data for dA-AAI adduct levels, cell viability as well as NQO1 expression and activity, hypothesized to be required for AAI bioactivation, in pHKC, HEK293 and RPTEC/TERT1 cells. Although dA-AAI adduct levels were significantly higher in differentiated RPTEC/TERT1 cells compared to HEK293 cells, we did not observe a difference in cell viability between the cell lines. Expression of hTERT can induce resistance to DNA-damaging response by suppression of p53-activation (Jin et al., 2010). However, the response of RPTEC/TERT1 to the DNA damaging substance B[a]P were deemed to be consistent with what is known regarding this cell type in a

normal, healthy kidney, including significant gene expression changes and induced BPDE-DNA adducts (Simon-Friedt et al., 2015). Moreover, we were able to detect dA-AAI adduct levels in RPTEC/TERT1 cells over the whole AAI-concentration range. The adduct levels were similar to levels found *in vivo* in rat tissue in our study and also in human patient material (Yun et al., 2012), indicating that the RPTEC/TERT1 cell systems represents a suitable model to investigate dA-AAI adduct formation in more detail. Interestingly, reduction of cell viability in the cell lines was not correlated to dA-AA adduct levels, suggesting either a cell-line specific bearable threshold in DNA-adducts, at which cells succumb to the damage, or DNA-independent toxicity of AAI. Substantial differences in activity of the involved DNA-repair pathway, i.e. nucleotide excision repair, can be ruled out as both RPTEC/TERT1 (Simon-Friedt et al., 2015) as well as HEK293 (Atanassov et al., 2004, Toga et al., 2014) are NER competent. Primary cells possess a similar gene expression profile to the originate cell type and present with, at least in the early passages, a relevant expression of organic anion transporters (OAT). OAT1 and OAT3 are major uptake transporters for AAI (Dickman et al., 2011, Xue et al., 2011) in proximal tubular epithelial cells and thus provide higher intracellular AAI levels. As expected, we determined the highest dA-AAI adduct levels and a most severely reduced cell viability in pHKC. Although we could not confirm OAT expression in our RPTEC/TERT1 cell model due to unavailability of an appropriate OAT antibody, Aschauer et al. (2014) demonstrated that the expression of organic anion transporters (OAT), mainly OAT1 and OAT3, are increased in differentiated RPTEC/TERT1 cells. Consistent with the data reported by Aschauer et al. (2014), we observed that dA-AAI adduct levels were higher in differentiated than in proliferating RPTEC/TERT1 cells.

Metabolic activation of AAI is required for the DNA adduct formation. It has been demonstrated that NQO1 is able to bioactivate AAI in cell free systems (Stiborova et al., 2011) and its role *in vivo* is also strongly suggested (Bárta et al., 2014). Indeed, Arlt et al. (Arlt et al., 2004) speculated that "*the detection of dA-AAI adducts in several organs of patients suggests*

the presence of AA activating enzymes in these organs and tissues and that AA and/or its metabolites are distributed via the bloodstream to other organs". Although the potential involvement of phase II metabolic enzymes as sulfotransferases (SULTs) appeared inconsistent (Meinl et al., 2006, Stiborova et al., 2011), nitroreduction followed by sulfation via SULT1B1 was demonstrated to further increase the mutagenic and cytotoxic potential of AAI (Sidorenko et al., 2014). In support of the latter, the most recent findings using primary human hepatocytes and renal proximal tubule epithelial cells in an organ-on-a-chip microphysiological system (Chang et al., 2017), reported aristolactam-N-sulfated ester (AL-I N-OSO_3) as the principle intermediate that would be formed in the hepatocytes and transported to the renal cortex to induce overt cytotoxicity and presumably formation of dA-AAI adducts. Based on the previous findings of Sidorenko et al. (2014) and Chang et al. (2017), demonstrating that hepatic phase II metabolism of the less reactive *N*-hydroxyaristolactam (AL-I-NOH) can lead to the formation of highly cytotoxic AL-I-N-OSO_3, immediate hepatoxicity would be expected either in the primary hepatocytes employed in the organ-on-a-chip application or in the patients affected. However, in neither of the exposure scenarios hepatotoxicity was reported (Yun et al., 2012, Arlt et al., 2004, Nortier et al., 2003) or shown in Chang et al. (2017). Thus, it appears questionable whether highly reactive metabolites can be metabolized and excreted from the liver without affecting the hepatic cells themselves, while entering the blood stream and exerting the toxic response in the kidney only. Rather, these findings suggest that metabolic activation of AAI primarily occurs in the renal cortex proper.

We investigated NQO1 expression in the human renal primary cells and cell lines and could not detect NQO1 expression or activity in HEK293, which correlated with the very low dA-AAI adduct formation. RPTEC/TERT1 cells expressed NQO1, showed high enzyme activity and also high adduct levels. In contrast, NQO1 expression and activity was low in pHKC, but dA-AAI adduct levels were highest of all human renal cells tested, even in comparison to

differentiated RPTEC/TERT1 at high AAI concentrations. Thus, while NQO1 activity followed expression levels, adduct formation did not. Continuous passaging of pHKC suggested increasing NQO1 activity (Fig S-6), which could be explained by an adaptive counteraction against oxidative stress (Dinkova-Kostova and Talalay, 2000). The observed variation of NQO1 in different passage numbers of pHKC demonstrated the highly variable phenotype of this cell model. AAI was not able to upregulate NQO1 activity in any of the applied renal cell systems, in contrast to the positive control sulforaphane, as expected (Brooks et al., 2001), but not in HEK293 devoid of NQO1. Consequently, we questioned the role of NQO1 as the only bioactivator of AAI in human renal cells. Indeed, it has been shown that also cytochrome P450 enzymes are able to activate AAI (Levová et al., 2011). Stiborova et al. (2012) demonstrated that human and rat CYPs detoxified AAI to 8-hydroxyaristolochic acid I (AAIa) via *O*-demethylation of the methoxy group, potentially resulting in a decreased renal toxicity (Xiao et al., 2008). However, the latter work focused mainly on CYP1a1/2, isoforms that are not expressed in human kidney (Knights et al., 2013). Other isoforms, such as human and rat CYPs of the 2C subfamily and human CYP3A4/5, 2D6, 2E1, and 1B1 also form AAIa but with much lower efficiency (Stiborová et al., 2015). Accordingly, while the role of CYP isoforms in AAI bioactivation is still under debate, CYPs may play a role especially in HEK293 cells showing absence of NQO1 expression. CYP mediated activation/detoxification highly depends on the aerobic conditions: anaerobic conditions promote AAI activation, while detoxifying *O*-demethylation is catalyzed at aerobic conditions, summarized by Stiborová et al. (2015).

Further investigations should therefore focus on the impact of the oxygen level on AAI DNA adduct formation and AAI induced toxicity. Indeed, cultivation at physiologically normal oxygen conditions for hepatic as well as renal cells, i.e. approx. 5% O_2 for the hepatocytes (Carreau et al., 2011) and 5-7% O_2 for the renal proximal tubule epithelial cells (Schiffer and Friederich-Persson, 2017), would provide for a much more realistic insight as to the

predominant pathways of AA metabolism and thus AAI DNA adduct formation and AAI induced toxicity.

In summary, we demonstrated a sensitive and reliable UPLC-MS/MS method to quantify dA-AAI adduct in DNA from human renal cell systems and tissue samples. We showed that RPTEC/TERT1 cells represented an appropriate model to investigate mechanism(s) underlying AAI-mediated DNA adduct formation in humans. In contrast, HEK293 may serve as excellent negative control to elucidate specific steps in metabolism of AAI in renal cells.

Acknowledgement

The authors thank Sabine Drewitz for technical support with the cell culture and Western Blot analysis. We thank the NMR Core facility at the University of Konstanz, especially Anke Friemel for the NMR data and Prof. Dr. Tanja Gaich for helpful assistance in the interpretation. We also thank the Proteomics Core facility at the University of Konstanz for the high-resolution MS data. Animal experiments were supported by the Federal Ministry of Education and Research (BMBF: 0313024). Mass spectrometric measurements were performed on an instrument funded by the German Research Foundation and the federal state of Baden-Wuerttemberg (DFG: INST 38/537-1). TZ was supported by a fellowship of the DFG-funded Graduate School ‘Konstanz Research School Chemical Biology (KoRS-CB, GSC 218).

References

Arlt, V.M., Alunni-Perret, V., Quatrehomme, G., Ohayon, P., Albano, L., Gaid, H., Michiels, J.F., Meyrier, A., Cassuto, E., Wiessler, M., Schmeiser, H.H., Cosyns, J.P., 2004. Aristolochic acid (AA)-DNA adduct as marker of AA exposure and risk factor for AA nephropathy-associated cancer. Int J Cancer 111, 977–980. https://doi.org/10.1002/ijc.20316

Aschauer, L., Carta, G., Vogelsang, N., Schlatter, E., Jennings, P., 2014. Expression of xenobiotic transporters in the human renal proximal tubule cell line RPTEC/TERT1. Toxicol. In Vitro. https://doi.org/10.1016/j.tiv.2014.12.003

Aschauer, L., Gruber, L.N., Pfaller, W., Limonciel, A., Athersuch, T.J., Cavill, R., Khan, A., Gstraunthaler, G., Grillari, J., Grillari, R., Hewitt, P., Leonard, M.O., Wilmes, A., Jennings, P., 2013. Delineation of the Key Aspects in the Regulation of Epithelial Monolayer Formation. Mol. Cell. Biol. 33, 2535–2550. https://doi.org/10.1128/MCB.01435-12

Atanassov, B., Velkova, A., Mladenov, E., Anachkova, B., Russev, G., 2004. Comparison of the global genomic and transcription-coupled repair rates of different lesions in human cells. Z. Naturforsch. C. 59, 445–453.

Bárta, F., Levová, K., Frei, E., Schmeiser, H.H., Arlt, V.M., Stiborová, M., 2014. The effect of aristolochic acid I on expression of NAD (P) H: quinone oxidoreductase in mice and rats—A comparative study. Mutat. Res. Toxicol. Environ. Mutagen. 768, 1–7. https://doi.org/http://dx.doi.org/10.1016/j.mrgentox.2014.01.012

Bieler, C.A., Stiborova, M., Wiessler, M., Cosyns, J.P., van Ypersele de Strihou, C., Schmeiser, H.H., 1997. 32P-post-labelling analysis of DNA adducts formed by aristolochic acid in tissues from patients with Chinese herbs nephropathy. Carcinogenesis 18, 1063–1067.

Brooks, J.D., Paton, V.G., Vidanes, G., 2001. Potent induction of phase 2 enzymes in human prostate cells by sulforaphane. Cancer Epidemiol. Biomarkers Prev. 10, 949–954.

Carreau, A., El Hafny-Rahbi, B., Matejuk, A., Grillon, C., Kieda, C., 2011. Why is the partial oxygen pressure of human tissues a crucial parameter? Small molecules and hypoxia. J. Cell. Mol. Med. 15, 1239–1253. https://doi.org/10.1111/j.1582-4934.2011.01258.x

Chang, S.-Y., Weber, E.J., Sidorenko, V.S., Chapron, A., Yeung, C.K., Gao, C., Mao, Q., Shen, D., Wang, J., Rosenquist, T.A., 2017. Human liver-kidney model elucidates the mechanisms of aristolochic acid nephrotoxicity. JCI insight 2.

Cosyns, J.-P., 2003. Aristolochic acid and "Chinese herbs nephropathy": a review of the evidence to date. Drug Saf. 26, 33–48. https://doi.org/10.2165/00002018-200326010-00004

Debelle, F.D., Vanherweghem, J.-L., Nortier, J.L., 2008. Aristolochic acid nephropathy: a worldwide problem. Kidney Int. 74, 158–169. https://doi.org/https://doi.org/10.1038/ki.2008.129

Depierreux, M., Van Damme, B., Vanden Houte, K., Vanherweghem, J.L., 1994. Pathologic aspects of a newly described nephropathy related to the prolonged use of Chinese herbs. Am J Kidney Dis 24, 172–180. https://doi.org/S0272638694001484 [pii]

Dickman, K.G., Sweet, D.H., Bonala, R., Ray, T., Wu, A., 2011. Physiological and Molecular Characterization of Aristolochic Acid Transport by the Kidney. J. Pharmacol. Exp. Ther. 338, 588–597. https://doi.org/10.1124/jpet.111.180984

Dinkova-Kostova, A.T., Talalay, P., 2000. Persuasive evidence that quinone reductase type 1 (DT diaphorase) protects cells against the toxicity of electrophiles and reactive forms of oxygen. Free Radic. Biol. Med. 29, 231–240. https://doi.org/https://doi.org/10.1016/S0891-5849(00)00300-2

Dong, H., Suzuki, N., Torres, M.C., Bonala, R.R., Johnson, F., Grollman, A.P., Shibutani, S., 2006. Quantitative determination of aristolochic acid-derived DNA adducts in rats using

32P-postlabeling/polyacrylamide gel electrophoresis analysis. Drug Metab Dispos 34, 1122–1127. https://doi.org/dmd.105.008706 [pii]10.1124/dmd.105.008706 [doi]

European Medicines Agency, 2011. Guideline on bioanalytical method validation. Comm. Med. Prod. Hum. Use.

Fahey, J.W., Dinkova-Kostova, A.T., Stephenson, K.K., Talalay, P., 2004. The "Prochaska" microtiter plate bioassay for inducers of NQO1, in: Methods in Enzymology. Elsevier, pp. 243–258. https://doi.org/https://doi.org/10.1016/S0076-6879(04)82014-7

FDA, U.S., 1995. Guideline for industry: text on validation of analytical procedures: ICH Q2A. Rockville, MD Mar 1, 995.

Goodenough, A.K., Schut, H.A.J., Turesky, R.J., 2007. Novel LC-ESI/MS/MSn Method for the Characterization and Quantification of 2 '-Deoxyguanosine Adducts of the Dietary Carcinogen 2-Amino-1-methyl-6-phenylimidazo [4, 5-b] pyridine by 2-D Linear Quadrupole Ion Trap Mass Spectrometry. Chem. Res. Toxicol. 20, 263–276. https://doi.org/10.1021/tx0601713

Houghton, C.A., Fassett, R.G., Coombes, J.S., 2016. Sulforaphane and Other Nutrigenomic Nrf2 Activators: Can the Clinician's Expectation Be Matched by the Reality? Oxid. Med. Cell. Longev. 2016, 7857186. https://doi.org/10.1155/2016/7857186

Jadot, I., Declèves, A.-E., Nortier, J., Caron, N., 2017. An Integrated View of Aristolochic Acid Nephropathy: Update of the Literature. Int. J. Mol. Sci. 18, 297. https://doi.org/10.3390/ijms18020297

Jelakovi, Cacute, B., Karanovi, Cacute, S., Vukovi, Cacute, I., Lela, F.M., Edwards, K.L., Nikoli, Cacute, J., Tomi, Cacute, K., Slade, N., Brdar, B., Turesky, R.J., 2011. Aristolactam-DNA adducts are a biomarker of environmental exposure to aristolochic acid. Kidney Int. 81, 559–567. https://doi.org/10.1038/ki.2011.371

Jin, X., Beck, S., Sohn, Y.-W., Kim, J.-K., Kim, S.-H., Yin, J., Pian, X., Kim, S.-C., Choi, Y.-J., Kim, H., 2010. Human telomerase catalytic subunit (hTERT) suppresses p53-

mediated anti-apoptotic response via induction of basic fibroblast growth factor. Exp. Mol. Med. 42, 574–582. https://doi.org/10.3858/emm.2010.42.8.058

Knights, K.M., Rowland, A., Miners, J.O., 2013. Renal drug metabolism in humans: the potential for drug-endobiotic interactions involving cytochrome P450 (CYP) and UDP-glucuronosyltransferase (UGT). Br. J. Clin. Pharmacol. 76, 587–602. https://doi.org/10.1111/bcp.12086

Levová, K., Moserová, M., Kotrbová, V., Šulc, M., Henderson, C.J., Wolf, C.R., Phillips, D.H., Frei, E., Schmeiser, H.H., Mareš, J., Arlt, V.M., Stiborová, M., 2011. Role of cytochromes P450 1A1/2 in detoxication and activation of carcinogenic aristolochic acid I: studies with the hepatic NADPH: cytochrome P450 reductase null (HRN) mouse model. Toxicol. Sci. 121, 43–56. https://doi.org/https://doi.org/10.1093/toxsci/kfr050

Meinl, W., Pabel, U., Osterloh‐Quiroz, M., Hengstler, J.G., Glatt, H., 2006. Human sulphotransferases are involved in the activation of aristolochic acids and are expressed in renal target tissue. Int. J. cancer 118, 1090–1097. https://doi.org/https://doi.org/10.1002/ijc.21480

Nortier, J.L., Martinez, M.C., Schmeiser, H.H., Arlt, V.M., Bieler, C.A., Petein, M., Depierreux, M.F., De Pauw, L., Abramowicz, D., Vereerstraeten, P., Vanherweghem, J.L., 2000. Urothelial carcinoma associated with the use of a Chinese herb (Aristolochia fangchi). N Engl J Med 342, 1686–1692. https://doi.org/10.1056/NEJM200006083422301 [doi]

Nortier, J.L., Schmeiser, H.H., Muniz Martinez, M.C., Arlt, V.M., Vervaet, C., Garbar, C.H., Daelemans, P., Vanherweghem, J.L., 2003. Invasive urothelial carcinoma after exposure to Chinese herbal medicine containing aristolochic acid may occur without severe renal failure. Nephrol Dial Transpl. 18, 426–428.

O'Brien, E., Heussner, A.H., Dietrich, D.R., 2001. Species-, sex-, and cell type-specific effects of ochratoxin A and B. Toxicol. Sci. 63, 256–264.

Pfau, W., Schmeiser, H.H., Wiessler, M., 1990. Aristolochic acid binds covalently to the exocyclic amino group of purine nucleotides in DNA. Carcinogenesis 11, 313–319. https://doi.org/https://doi.org/10.1093/carcin/11.2.313

Schiffer, T.A., Friederich-Persson, M., 2017. Mitochondrial Reactive Oxygen Species and Kidney Hypoxia in the Development of Diabetic Nephropathy. Front. Physiol. 8, 211. https://doi.org/10.3389/fphys.2017.00211

Sidorenko, V.S., Attaluri, S., Zaitseva, I., Iden, C.R., Dickman, K.G., Johnson, F., Grollman, A.P., 2014. Bioactivation of the human carcinogen aristolochic acid. Carcinogenesis 35, 1814–1822. https://doi.org/https://doi.org/10.1093/carcin/bgu095

Sidorenko, V.S., Yeo, J.E., Bonala, R.R., Johnson, F., Scharer, O.D., Grollman, A.P., 2012. Lack of recognition by global-genome nucleotide excision repair accounts for the high mutagenicity and persistence of aristolactam-DNA adducts. Nucleic Acids Res 40, 2494–2505. https://doi.org/10.1093/nar/gkr1095

Simon-Friedt, B.R., Wilson, M.J., Blake, D.A., Yu, H., Eriksson, Y., Wickliffe, J.K., 2015. The RPTEC/TERT1 cell line as an improved tool for in vitro nephrotoxicity assessments. Biol. Trace Elem. Res. 166, 66–71. https://doi.org/10.1007/s12011-015-0339-y

Stemmer, K., Ellinger-Ziegelbauer, H., Ahr, H.J., Dietrich, D.R., 2007. Carcinogen-specific gene expression profiles in short-term treated Eker and wild-type rats indicative of pathways involved in renal tumorigenesis. Cancer Res 67, 4052–4068. https://doi.org/67/9/4052 [pii]10.1158/0008-5472.CAN-06-3587

Stiborová, M., Arlt, V.M., Schmeiser, H.H., 2017. DNA Adducts Formed by Aristolochic Acid Are Unique Biomarkers of Exposure and Explain the Initiation Phase of Upper Urothelial Cancer. Int. J. Mol. Sci. 18, 2144. https://doi.org/10.3390/ijms18102144

Stiborová, M., Bárta, F., Levová, K., Hodek, P., Schmeiser, H.H., Arlt, V.M., Martínek, V., 2015. A Mechanism of O-Demethylation of Aristolochic Acid I by Cytochromes P450

and Their Contributions to This Reaction in Human and Rat Livers: Experimental and Theoretical Approaches. Int. J. Mol. Sci. 16, 27561–27575. https://doi.org/10.3390/ijms161126047

Stiborova, M., Frei, E., Arlt, V.M., Schmeiser, H.H., 2009. The role of biotransformation enzymes in the development of renal injury and urothelial cancer caused by aristolochic acid: urgent questions and difficult answers. Biomed. Pap. Med. Fac. Palacky Univ. Olomouc 153. https://doi.org/DOI: 10.5507/bp.2009.001

Stiborova, M., Frei, E., Hodek, P., Wiessler, M., Schmeiser, H.H., 2005. Human hepatic and renal microsomes, cytochromes P450 1A1/2, NADPH:cytochrome P450 reductase and prostaglandin H synthase mediate the formation of aristolochic acid-DNA adducts found in patients with urothelial cancer. Int J Cancer 113, 189–197. https://doi.org/10.1002/ijc.20564 [doi]

Stiborova, M., Frei, E., Sopko, B., Sopkova, K., Markova, V., Lankova, M., Kumstyrova, T., Wiessler, M., Schmeiser, H.H., 2003. Human cytosolic enzymes involved in the metabolic activation of carcinogenic aristolochic acid: evidence for reductive activation by human NAD(P)H:quinone oxidoreductase. Carcinogenesis 24, 1695–1703. https://doi.org/10.1093/carcin/bgg119bgg119 [pii]

Stiborova, M., Levova, K., Barta, F., Shi, Z., Frei, E., Schmeiser, H.H., Nebert, D.W., Phillips, D.H., Arlt, V.M., 2012. Bioactivation versus detoxication of the urothelial carcinogen aristolochic acid I by human cytochrome P450 1A1 and 1A2. Toxicol. Sci. 125, 345–358. https://doi.org/10.1093/toxsci/kfr306

Stiborova, M., Mareis, J., Frei, E., Arlt, V.M., Martinek, V., Schmeiser, H.H., 2011. The human carcinogen aristolochic acid i is activated to form DNA adducts by human NAD(P)H:quinone oxidoreductase without the contribution of acetyltransferases or sulfotransferases. Env. Mol Mutagen 52, 448–459. https://doi.org/10.1002/em.20642

Toga, T., Kuraoka, I., Watanabe, S., Nakano, E., Takeuchi, S., Nishigori, C., Sugasawa, K.,

Iwai, S., 2014. Fluorescence detection of cellular nucleotide excision repair of damaged DNA. Sci. Rep. 4, 5578. https://doi.org/10.1038/srep05578

Wieser, M., Stadler, G., Jennings, P., Streubel, B., Pfaller, W., Ambros, P., Riedl, C., Katinger, H., Grillari, J., Grillari-Voglauer, R., 2008. hTERT alone immortalizes epithelial cells of renal proximal tubules without changing their functional characteristics. AJP Ren. Physiol. 295, F1365–F1375. https://doi.org/10.1152/ajprenal.90405.2008

Xiao, Y., Ge, M., Xue, X., Wang, C., Wang, H., Wu, X., Li, L., Liu, L., Qi, X., Zhang, Y., Li, Y., Luo, H., Xie, T., Gu, J., Ren, J., 2008. Hepatic cytochrome P450s metabolize aristolochic acid and reduce its kidney toxicity. Kidney Int 73, 1231–1239. https://doi.org/ki2008103 [pii]10.1038/ki.2008.103 [doi]

Xue, X., Gong, L.-K., Maeda, K., Luan, Y., Qi, X.-M., Sugiyama, Y., Ren, J., 2011. Critical role of organic anion transporters 1 and 3 in kidney accumulation and toxicity of aristolochic acid I. Mol. Pharm. 8, 2183–2192. https://doi.org/10.1021/mp100418u

Yun, B.H., Rosenquist, T.A., Sidorenko, V., Iden, C.R., Chen, C.-H., Pu, Y.-S., Bonala, R., Johnson, F., Dickman, K.G., Grollman, A.P., Turesky, R.J., 2012. Biomonitoring of Aristolactam-DNA Adducts in Human Tissues Using Ultra-Performance Liquid Chromatography/Ion-Trap Mass Spectrometry. Chem. Res. Toxicol. 25, 1119–1131. https://doi.org/10.1021/tx3000889

Yun, B.H., Xiao, S., Yao, L., Krishnamachari, S., Rosenquist, T.A., Dickman, K.G., Grollman, A.P., Murugan, P., Weight, C.J., Turesky, R.J., 2017. A Rapid Throughput Method To Extract DNA from Formalin-Fixed Paraffin-Embedded Tissues for Biomonitoring Carcinogenic DNA Adducts. Chem. Res. Toxicol. 30, 2130–2139. https://doi.org/10.1021/acs.chemrestox.7b00218

Figure Caption

Fig. 1: Presumed metabolic activation of AAI/AAII in human cell systems. AA is activated via enzymatic nitro-reduction (e.g. via NQO1) to *N*-hydroxy-aristolactam. Further metabolization by a yet unknown pathway leads to the highly reactive nitrenium/carbenium ion, which is able to bind to DNA and leads to the formation of dA-AAI/II and dG-AAI/II adducts.

Fig. 2: Product ion spectra of (a) dA-AAI (*m/z* 543) and (b) [$^{15}N_5$]-dA-AAI (*m/z* 548), representing (c) the fragmentation of the adducts. Major fragments detected by UPLC-MS/MS were the aglycone base adducts upon loss of the deoxyribose (dA-AAI $[BH_2]^+$ (*m/z* 427) and [$^{15}N_5$]-dA-AAI $[BH_2]^+$ (*m/z* 432)). (d) Linearity of the standard curves used for adduct quantification. The coefficient of determination (r^2) of the slopes were ≥ 0.99. (e-f) Mass chromatograms of AAI modified genomic DNA. Peak areas at retention time (t_R) of 4.2 min for dA-AAI (*red*) and [$^{15}N_5$]-dA-AAI (*blue*) were analyzed from (e) control or (f) 50 µM AAI exposed differentiated RPTEC/TERT1 cells.

Fig. 3: Time-dependent increase in dA-AAI adduct formation and bodyweight reduction in AAI/II treated EKER rats. (a-d) Quantification of dA-AAI adduct formation in DNA from kidney cortex (a, b) and bladder (c, d) in male and female EKER rats after 1, 3, 7 and 14 days of AAI/II (10 mg/kg body weight) (*black*) or control treatment (*grey*). Values represent mean ± SEM of n=3 (male and female kidney cortex ctrl. d14 only n=2). (e-f) Observed differences in bodyweight (bw) of the EKER rats calculated by subtraction of the bw at d0 from bw at time of sacrifice. Bw changes were analyzed for AAI/II (*black*) or control treated (*grey*) male and female EKER rats. Values above *y=0* represent an increase in bw, values below *y=0* represent a loss in bw. Values are presented in a box-and-whisker plot with whiskers indicating min and max values (n=3). Statistical significance was analyzed using 2-way ANOVA with Sidak's multiple comparison test and * indicates *p*-value ≤ 0.05, ** indicates *p*-value ≤ 0.0001.)

Fig. 4: Quantification of dA-AAI adducts and cell viability in human renal cell types after 48h AAI exposure. AAI DNA adduct levels were compared in (a) HEK293 *(red)*, differentiated RPTEC/TERT1 *(black)* and pHKC *(blue)* cells or (b) in proliferating *(green)* or differentiated *(black)* RPTEC/TERT1 cells cultured on 2D wells or cultured on transwell inserts *(magenta)*. Values represent mean ± SEM of n=3. Statistics: 2-way ANOVA followed by a Tukey's post-test,* indicates *p*-value ≤ 0.0001. (c) Cell viability in was analyzed in HEK293 *(red)*, differentiated RPTEC/TERT1 *(black)* and pHKC *(blue)* cells. Values represent mean ± SEM. Statistics: 2-way ANOVA followed by a Tukey's post-test, * indicates *p*-value ≤ 0.0001. (d) Cell viability was compared to dA-AAI adduct levels in HEK293 *(red)*, differentiated RPTEC/TERT1 *(black)* and pHKC *(blue)* cells.

Fig. 5: Activity and expression analysis of NQO1 in human renal cell systems. (a) Representative image of Western Blot analysis used for quantification using specific antibodies for human NQO1 (31 kDa) and β-actin (loading control, 42 kDa) in HEK293, proliferating and differentiated RPTEC/TERT1 cells cultured on plastic or on transwell inserts and pHKC cells. (b) Quantification of Western Blot analysis of NQO1 expression normalized to β-actin expression. Dashed line indicates background-level, not significantly different from zero. Values represent mean ± SEM in n=3. Statistical significance was analyzed using 1-way ANOVA with Tukey's multiple comparison test and * indicates *p*-value ≤ 0.05. Expression levels of pHKC was compared to background level with an unpaired t test and *a* in indicates *p*-value ≤ 0.01 (c) Quantification of specific NQO1 enzyme activity in the same cell systems. Specific NQO1 activity was normalized to total protein amount. Dashed line indicates background-level, not significantly different from zero. Values represent mean ± SEM in n=3. Statistical significance was analyzed using 1-way ANOVA with Tukey's multiple comparison test and * indicates *p*-value ≤ 0.001. Activity levels of pHKC was compared to background level with an unpaired t test and *a* in indicates *p*-value ≤ 0.05 (d) NQO1 activity normalized to

NQO1 expression level. Dashed line indicates background-level, not significantly different from zero. Statistical significance was analyzed using 1-way ANOVA with Tukey's multiple comparison test and * indicates p-value ≤ 0.05.

Fig. 6: Comparison of specific NQO1 activity after AAI treatment for 48h in differentiated RPTEC/TERT1 (a), HKC (b) and HEK293 (c) cells. For positive control, cells were treated for 48h with sulforaphane (5µM). Specific NQO1 activity was normalized to total protein amount. Values represent mean ± SEM. Statistical significance was analyzed using 1-way ANOVA with Tukey's multiple comparison test and * indicates p-value ≤ 0.01.

Fig 1

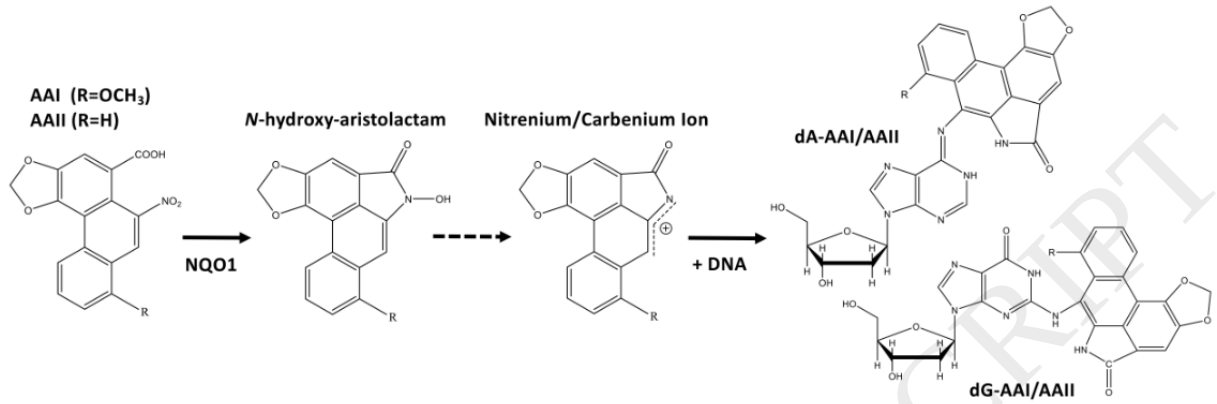

Fig 2

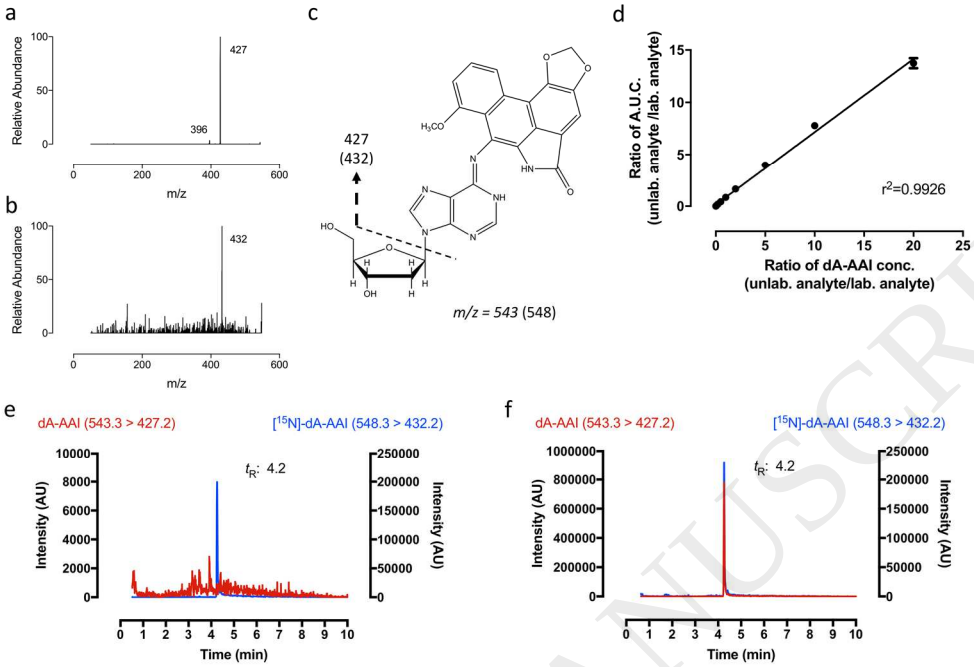

Fig 3

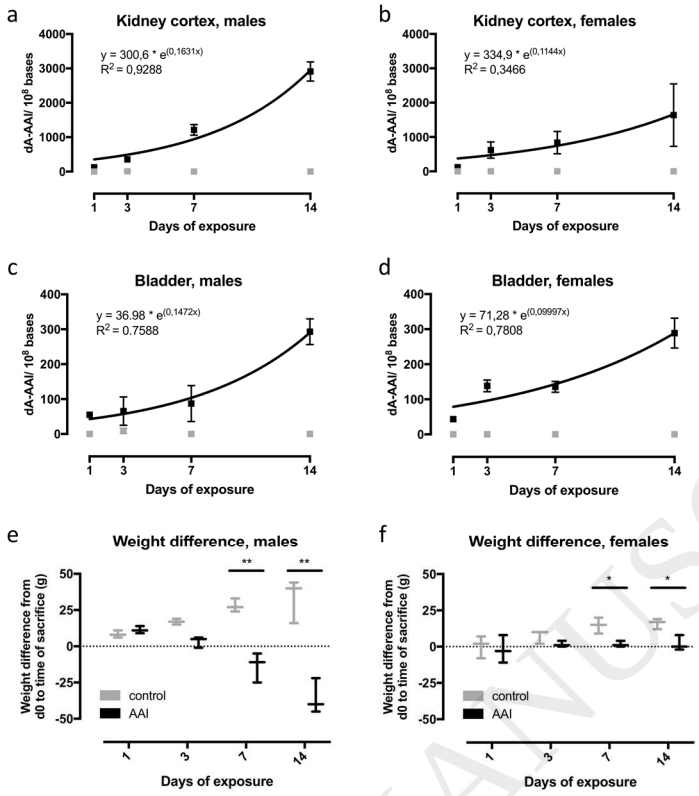

Fig 4

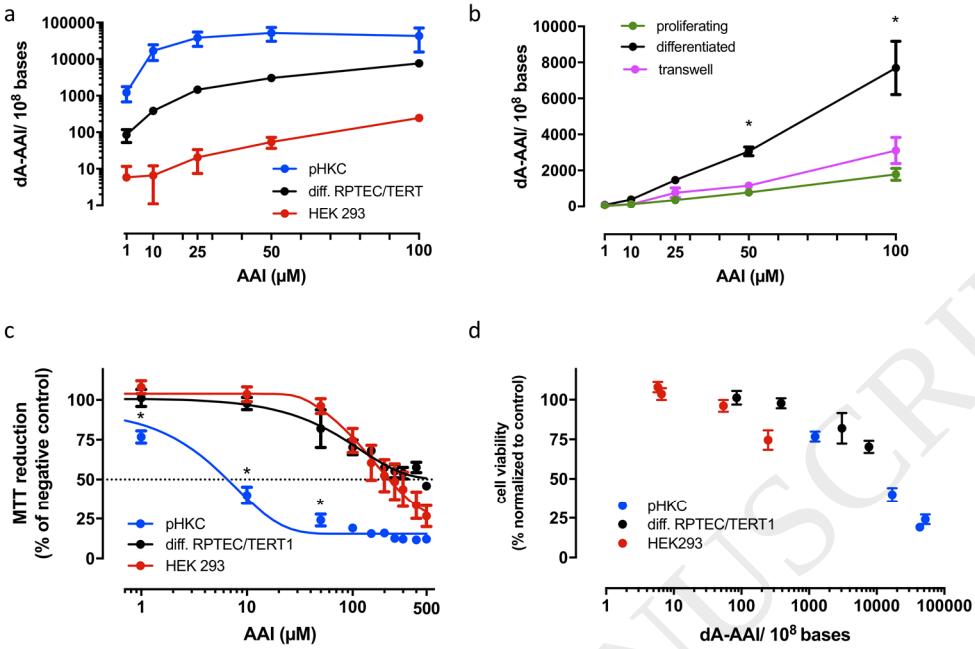

Fig 5

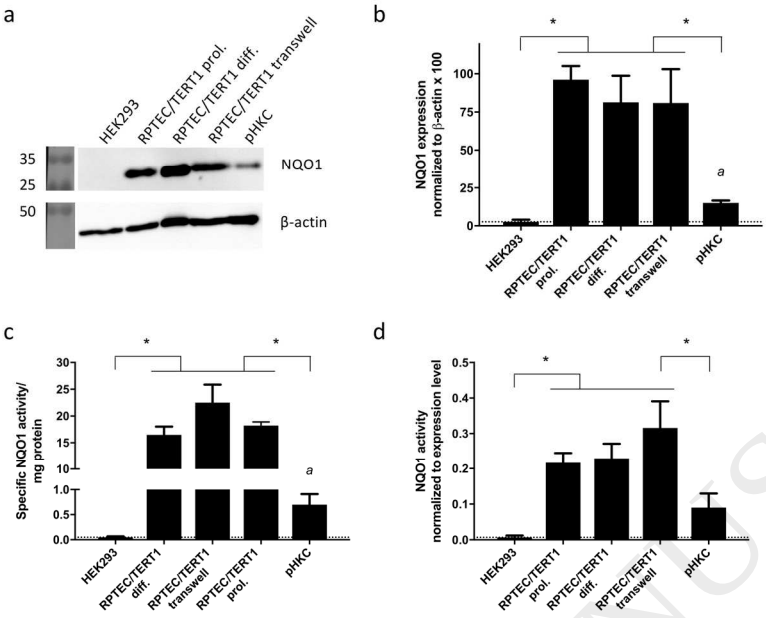

Fig 6

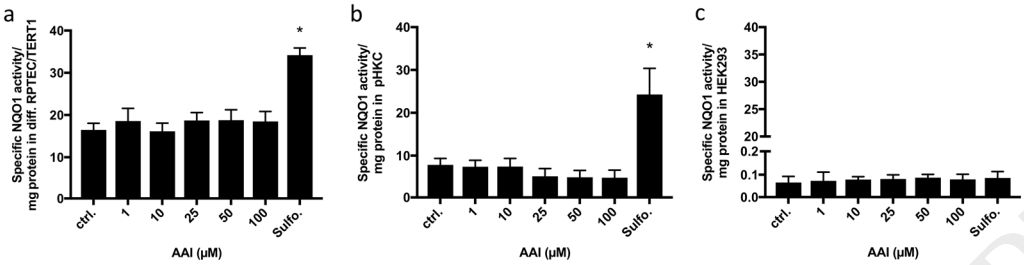

Table 1: Linearity and sensitivity of the mass spectrometric method for quantification of dA-AAI adducts.

	Linear range [fmol]	Calibration curve (n=3)	Linearity (r^2)	LLOD [fmol]	LOQ [fmol]
dA-AAI	1-1000	y = (0.6994±0.01141)x + (0.1612±0.08306)	0.9926	0.1	0.5

Table 2: Validation parameters of the mass spectrometric method for quantification of dA-AAI adducts.

		Recovery [%]	Matrix effect [%]	Precision [% RSD]	
		(n=3)	(n=3)	Interday (n=5)	Intraday (n=5)
dA-AAI	LQC	95.3	95.3	11.9	13.1
	MQC	101.4	107.4	9.1	10.7
	HQC	93.8	103.1	8.9	9.8

Table 3: Stability determination of dA-AAI adducts.

		Freeze-Thaw [%RSD]	Short-term storage [% RSD]		Long-term storage [% RSD]	
			RT (n=3)	37°C (n=3)	-20°C (n=3)	-80°C (n=3)
dA-AAI	LQC	2.9	1.1	1.7	1.2	1.5
	MQC	1.0	0.8	0.6	1.8	0.6
	HQC	0.2	0.5	0.6	1.0	1.3